IEEE Access
Multidisciplinary | Rapid Review | Open Access Journal

Received 22 January 2025, accepted 7 February 2025, date of publication 13 March 2025, date of current version 24 March 2025.

Digital Object Identifier 10.1109/ACCESS.2025.3548976

RESEARCH ARTICLE

Simulation-Based Investigation of Wind Turbine Induced Shadow Flicker on IGBT Reliability and Energy Yield in Solar Converters in Hybrid Wind-Solar Systems

LEANDER VAN CAPPELLEN[1,2,3], MARTIJN DECKERS[3,4], (Graduate Student Member, IEEE), KRISTOF ENGELEN[3,4], GEORGI H. YORDANOV[3,4], AND MICHAËL DAENEN[1,2,3]

[1]Institute for Materials Research (IMO-IMOMEC), Hasselt University, 3500 Hasselt, Belgium
[2]IMEC, IMO-IMOMEC, 3590 Diepenbeek, Belgium
[3]IMO-IMOMEC, Energy Ville, 3600 Genk, Belgium
[4]Department Elektrotechniek/Department of Electrical Engineering, KU Leuven, 3001 Heverlee, Belgium

Corresponding author: Leander Van Cappellen (leander.vancappellen@uhasselt.be)

This work was supported by the Belgian Energy Transition Funds/Met de steun van het Energietransitiefonds.

ABSTRACT With the growing adoption of renewable energy, hybrid wind-solar plants are gaining interest because they allow the increase of energy yield per unit of surface area. However, the presence of wind turbines creates unique shading scenarios for the solar panels. This work presents a simulation-based approach to investigate the solar plant's energy yield and converter IGBT lifetime in the presence of dynamic and fast-moving shadows created by the wind turbine blades. First, the need for a dynamic simulation as opposed to a static one is examined. Next, the sensitivity of Photovoltaic (PV) string orientation, PV string location, wind direction, Maximum Power Point Tracker (MPPT) control speed, and turbine rotor speeds on energy yield and IGBT lifetime are investigated in a case study. Results show that dynamic and static simulations can show vastly different results. MPPT can have difficulty with shadow flicker, resulting in different string voltages depending on the MPPT update speed and wind turbine rotor speed. The shadow flicker introduces additional temperature swings in the IGBT, but these are too small to add any significant lifetime consumption ($< 1.2\%$). Thus, the observed changes in lifetime consumption are caused mainly by controller behavior and static shadows. Finally, it is concluded that PV strings are better placed south, east, or west of the wind turbine for optimal energy yield and lifetime consumption. A northern placement can be suitable if there is a significant distance (+50 m) between the PV string and the wind turbine.

INDEX TERMS Dc-dc power converters, lifetime estimation, solar energy, solar panels, wind turbines, yield estimation.

I. INTRODUCTION

The energy transition to renewable energy sources results in the construction of an increasing number of solar and wind turbine installations. In 2023, solar and wind energy were responsible for 5.5% and 7.8% of total global electric energy generation, respectively [1]. Unfortunately, space is not always plentiful. Because of this, wind and photovoltaic (PV) installations can be combined to maximize the use of available space and minimize system costs [2], [3], [4]. These hybrid wind and PV installations create unique operating conditions for both PV panels and converters because the wind turbines will cast a systematic shadow on the panels. This shadow consists of two parts: the shadow of the turbine tower and the rotor blades. The tower will produce a slowly moving shadow while the shadow cast by rotor blades causes a shadow flicker on the panels below and thus causes frequent power fluctuations in the PV system. These power

The associate editor coordinating the review of this manuscript and approving it for publication was Yuh-Shyan Hwang.

fluctuations can lead to decreased energy yield and additional stress on both PV cells and the internal components of the converter. One of the most failure-prone components in PV converters is the switching device [5]. They experience thermal, electrical, and environmental stress in their lifetime, which can result in wear-out failure like die attach cracks, bond wire cracks, and bond wire liftoff [6], [7]. Hence, in the case of a hybrid wind and PV installation, frequent power fluctuations can result in additional thermo-mechanical stress and reduce the lifetime of the system.

Research towards modeling of wind turbine-induced shadow in PV systems has already been performed [8], [9], [10], [11], [12], [13]. They, however, are focused on plant efficiency and ignore the dynamic movement of the rotor blades. Dekker et al. have conducted a study that measured the effect of dynamic shading of the wind turbine on the performance of the PV system [14]. They found that dynamic shading by wind turbines can significantly affect power generation due to the non-optimal configuration of the Maximum Power Point Tracker (MPPT) and inverter control. The study only performs measurements and does not try to replicate the system behavior in a model. Studies on how wind turbines can influence converter lifetime are lacking.

This paper will focus on developing a methodology to dynamically simulate the hybrid wind PV installation, taking turbine rotor rotation into account. Using the developed methodology a case study will be conducted to investigate the following research questions:

- What is the impact of wind turbine-induced shadow flicker on IGBT licensed shadow flicker on IGBT lifetime and solar energy yield?
- Is there preferential placement of solar arrays in wind-solar parks?

The Unity engine is used to build a virtual, hybrid solar and wind installation. The model simulates realistic operating conditions by accounting for the sun's position and the precise movement of the wind turbine rotor. Next, the string voltage and current can be used to calculate PV system energy yield. The thermal load profile of the IGBT junction can be used to evaluate the wear-out failure. This evaluation will be performed for multiple string orientations, string locations, wind turbine rotation speeds, and converter MPPT update speeds for a real one-year solar mission profile.

The paper is structured as follows: section II will discuss the used methodology and explain the used electrical, PV, control, thermal, Unity model, and lifetime models. Section III will discuss results for all different cases, and section IV will end with a conclusion.

II. METHODOLOGY

A. 3D SOLAR-WIND PLANT SIMULATION

To capture the shading cast by a wind turbine as realistically as possible, a complete hybrid solar-wind plant needs to be simulated. Unity is widely used as a game engine, but because of its built-in functions to place objects, simulate movement, and track collisions, it is perfect for simulating the hybrid plant.

The scene contains three components, as shown in Fig. 1: the turbines, sun, and PV modules. The sun is simulated as a point in space 150 million km away from the park. With date, time, and geographic location on Earth, the current location of the sun in the sky can be calculated. This way, the sun can be moved through the sky while the plant stays still to mimic the behavior of the earth's rotations and rotation of the earth around the sun.

Typically, a PV module has 60 or more cells, but because of the scale and computation time of the model, it is not feasible to simulate each cell. Therefore, it is assumed that each module contains three sub-strings of 6 cells each and one bypass diode per sub-string. Each cell in the PV modules has 2 states: shaded or not shaded. Each cell has thus its own unique shade mission profile. The model simulates time from January 1, 2023, to December 31 2023. To accurately capture the effect of shadow flicker on the modules, the time resolution needs to be high. This would require an unacceptable amount of computational power, so some methods are introduced to reduce the computation time. Firstly, because the sun's apparent movement through the sky is quite slow, the shadows are measured every 5 minutes. During the measurement, the time resolution is kept at 0.02 s. Secondly, the measurement duration is taken as the time needed to complete a 120° rotation of the turbine rotor. This data can then be repeated during data processing to create a full 5-minute interval of shade data at 0.02 s resolution. The measurement is performed by using the ray-cast function of Unity. The ray is cast from the sun to each of the PV cells. If the ray collides with the mesh of the wind turbine, a collider flag will trigger and the cell will be considered shaded. This is done for each time step to construct a shade profile for each individual cell.

B. PHOTOVOLTAIC MODEL

In this study, a single string of 28 PV panels is considered. As explained in section II-A, each panel contains three sub-strings of 6 cells each. This results in a total of 504 cells. Each cell has two potential states: shaded or not shaded. When the cell is not shaded, it is exposed directly to the open sky and thus receives global horizontal irradiance. When the cell is shaded, only diffuse light is hitting the cell. When the wind turbine casts a shadow on the PV array, the number of shaded cells changes constantly. This means that the IV curve of the PV system changes continuously and rapidly. It is important to correctly simulate the full PV string, including bypass diodes, to provide a realistic PV string voltage and current input for the converter. In order to accomplish this, each cell and diode does not need to be simulated discretely, but they can be grouped together. The cells can be divided into three groups:

- Group 1: Cells in sub-string where no cell is shaded.

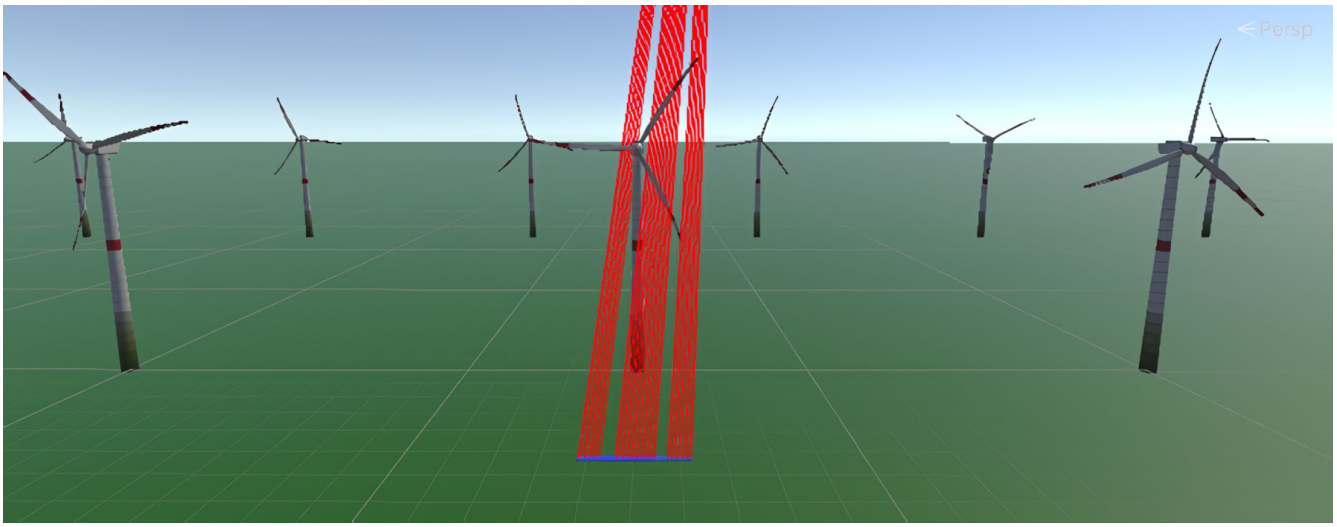

FIGURE 1. Unity scene with three elements: wind turbines, PV array, and sun. The ray-cast (in red) from the sun to cells is blocked by the wind turbine for some cells.

- Group 2: Cells in sub-strings that contain shaded cells but are themselves not shaded
- Group 3: Cells that are shaded.

Fig. 2 shows the simplified equivalent circuit of the complete PV array. All cells are placed in series in their corresponding group. In this study, the string IV-curve will be constructed by combining the individual cell IV-curves. When some cells are shaded, there are two regions in the IV curve, as shown in Fig. 3. In the first part of the curve, group 1 produces more current than group 3, activating the bypass diode. This leads to zero voltage across the sub-strings with cells of groups 2 and 3 when the diodes are assumed to be ideal. Because the cells in group 2 are in series with cells from group 3, they will also not generate power. In this area of the IV-curve, only the cells from group 1 contribute. Hence the string IV-curve can be constructed by multiplying the voltage of the IV curve of a group one cell by the amount of group one members. In the second part of the curve, the current drops enough so the bypass diodes are not active. This results in a series connection of all the cells. Consequently, the string IV-curve can be constructed by the sum of all cell IV-curves along the voltage axis.

C. CONTROL

The voltage and current of the string are determined by both environmental factors, like irradiance and shade, and the inverter controller behavior. This voltage and current directly determine the losses in the IGBT and, thus, the junction temperature. It is crucial to determine how the converter controller reacts to sudden shading conditions and how this affects string voltage and current. Dekker et al. reported current drops when dynamic shading is introduced [14]. The converter attempts to maintain stable string voltage. However, due to variations in the MPPT algorithm, step size, and overshoot, voltage fluctuations and offsets may occur. To further validate this, a small-scale experiment was conducted to observe how the converter responds to dynamic shading.

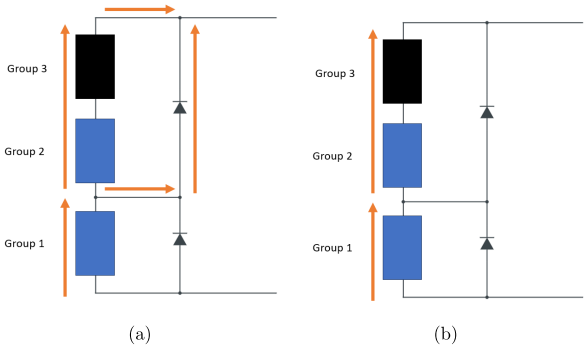

FIGURE 2. String current flow in (a) Bypass active and (b) Bypass not active.

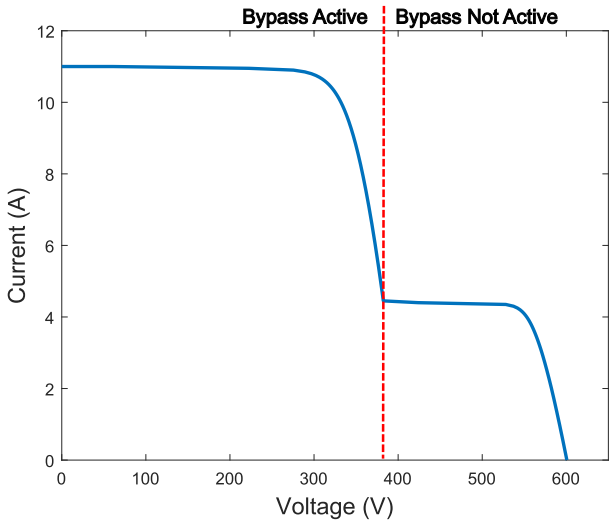

FIGURE 3. IV curve of partial shaded PV string.

In the experiment, a single PV panel in a string is quickly covered and uncovered to mimic a quick passing shading event. The setup consists of a south-oriented and north-oriented string with each 13 panels in series. Each string is connected to separate MPPT inputs on an ABB Trio 8.5 kW inverter. Only the southern string is used for the shading experiment. The string voltage and current are measured near the inverter input with a National Instrument DAQ setup at a resolution of 40 μs.

A single PV panel is manually covered with a tarpaulin to mimic a sudden partial shading event and is removed after a couple of seconds. The results are shown in Fig. 4. The experiment can be split into 4 sequential events, which are visible on the IV-curve and measurement data:

1) Shadow is introduced. String voltage stays constant while the current drops.
2) MPPT searches the new MPP by dropping string voltage.
3) Shadow is removed. String voltage stays constant while current rises.
4) MPPT starts increasing string voltage to reduce current and regain initial MPP.

It is clear that the inverter keeps the voltage constant in a shading event. This results in an extreme current drop over a period of 0.13 s. Note that the application of shade was a manual process; thus, a faster shading event could result in an even faster current drop. Similar results are seen when the shadow is removed. For the simulation, the main takeaway is that the inverter keeps the input voltage constant and drops the current according to the IV curve. The experiment shows this drop is fast, and because the MPPT update speed does not drop below 0.02 s in this study, it is assumed to be instantaneous. Another observation is a noticeable voltage ripple, caused by the MPPT searching for a new maximum at approximately 10 V/s.

In this study, MPPT control is simulated completely separate from the electrical model. The simulated MPPT controller moves the MPP on the IV curve to determine the instantaneous string voltage and current. This voltage and current can later be used in the electrical model. There are various MPPT algorithms available [15], including: perturb and observe (P&O) [16], incremental conductance [17], hill climbing [18], current sweep [19], ripple correlation control [20], extremum seeking control [21], PSO and neural network based MPPT [22], …Each MPPT algorithm and control implementation can result in possible different reaction of the converter to dynamic shading. For this study, a perturb and observe (P&O) algorithm is chosen for the MPPT. The MPPT takes voltage steps of 1 V and has a variable update speed depending on the studied case. Because P&O algorithms can get stuck in local maxima, a complete IV-sweep is performed every 6 min to find the true global maximum. The IV sweep takes 0.5 s to complete. Fig. 5 shows an overview of the complete simulation loop. This loop is executed every 20 ms.

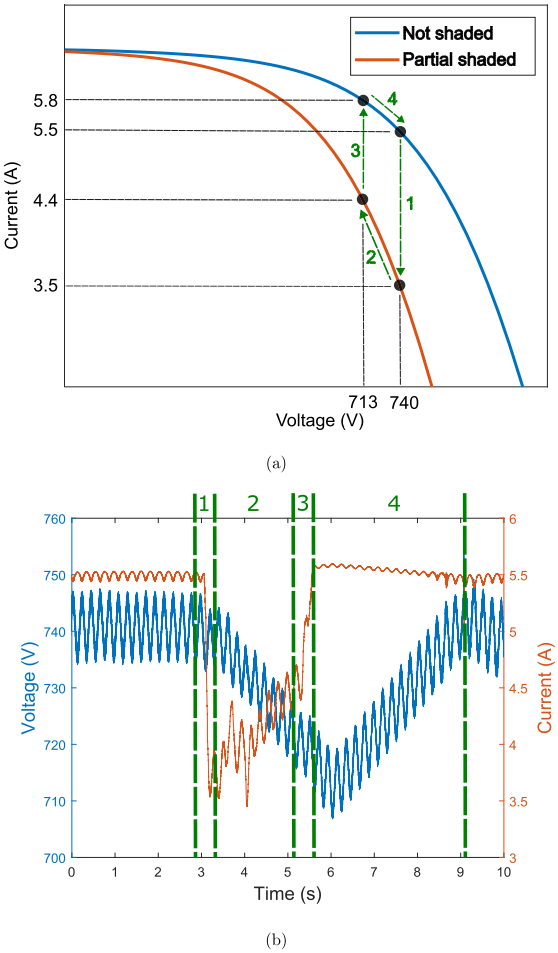

FIGURE 4. (a) Movement of power point on IV curves of non-shaded and partially shaded PV string in the experiment. (b) PV string voltage and current measured at inverter input during the experiment.

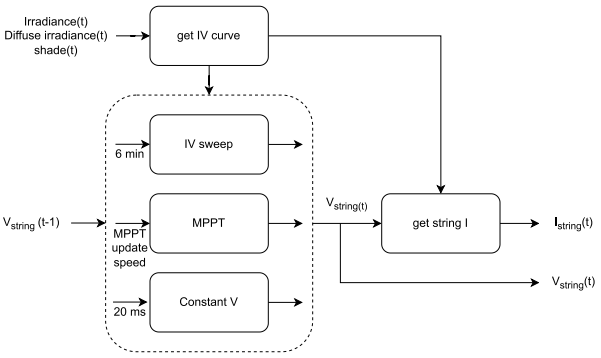

FIGURE 5. Simulation loop to calculate string voltage and current, this loop is executed at the 20 ms update speed.

D. ELECTRICAL MODEL

The converter in this study is a simple boost topology, as shown in Fig. 6. The output of the converter is connected to a 1000 V DC bus. The losses inside the IGBT can be approximated with equation 1 and 2.

$$P_{conduction} = DI_{in}^2 R_{on} \tag{1}$$

$$P_{switch} = \frac{1}{2} V_{out} I_{in} (t_{rise} + t_{fall}) f \tag{2}$$

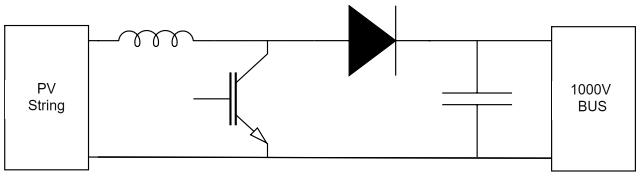

FIGURE 6. Boost converter topology.

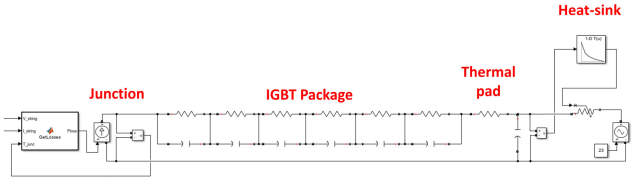

FIGURE 7. Electric and thermal model implemented in Matlab.

where V_{out} and I_{in} are the instantaneous output voltage and input current respectively, f the switching frequency (20 KHz) and D the duty cycle. The rise time t_{rise}, fall time t_{fall}, and the on-resistance R_{on} dependency on junction temperature and voltage are extracted from the datasheet. The chosen IGBT is the Infineon IKZA40N120CS7, which is described as an adequate IGBT for PV applications.

E. THERMAL MODEL

In this work, the thermal RC network, as shown in Fig. 7, is used to model the thermal path from the IGBT junction to ambient. The thermal model consists of multiple sections. Firstly, on the left is the electrical model, which feeds its losses into the thermal model. There is a feedback loop for the junction temperature to the electrical model to calculate the temperature-dependent R_{on} of the IGBT. Next, the heat will flow through the different packaging layers of the IGBT. These layers are modeled with a thermal foster network. The Foster parameters are extracted from the data sheet provided by the manufacturer. The final part of the thermal model consists of the thermal pad and heatsink. A Cauer network is used because Cauer layers represent physical material layers. The pad has a value of 0.85 K/W. The thermal capacitance and resistance of the heat sink can have a substantial impact on lifetime predictions [23]. A passive heat sink is designed to keep the junction temperature under 125 °C at all times. A fluid Finite Element Simulation is used to calculate the thermal resistance for multiple heat sink temperatures to create a lookup table [24]. The heat sink is then implemented as a variable thermal resistor, whose value changes depending on the heat sink temperature.

The thermal capacitance is determined to be 21.2 J/K using specific heat capacitance and heat sink size. Finally, the ambient temperature is kept to 23 ° during this study.

F. LIFETIME EVALUATION

In general, it is widely accepted that cyclic loading has a big impact on the IGBT package lifetime. Cyclic failure can be classified into two groups depending on the cycles to failure: under 10000 cycles to failure is considered low cycle fatigue, and everything above 10000 cycles is considered high cycle fatigue [25]. In low-cycle fatigue, plastic deformation is the dominant reason for failure. It happens in situations where the component is exposed to high load swings. It is often described using the Coffin-Manson relation. High cycle fatigue is caused by elastic deformation and is described by Basquin's relation. Most lifetime models are focused on low-cycle fatigue because it is often more dominant than high-cycle fatigue and considerably easier to perform in accelerated power cycling tests. In this study, the majority of the solar mission profile will result in plastic deformation and low cycle fatigue. However, the presence of shadow flicker will introduce a lot of smaller load cycles, which are possibly mainly elastic.

This introduction of large amounts of elastic cycles eliminates physics-based methods that evaluate lifetime with cumulative plastic energy because elastic deformation does not introduce energy loss. Additionally, physics-based methods are computationally expensive, which is not ideal for simulating long mission profiles [26], [27].

Another option lies with the analytical lifetime models where power cycling is performed to measure the number of cycles to failure [28]. In these tests, usually, high-temperature swings are applied to keep the test duration manageable. Using these models for high cycle fatigue would require extreme extrapolation and introduce significant error because of the transition from Coffin-Manson to Basquin. Fortunately, the popular CIPS08 model has been extended for lower temperature swings, which makes it suitable for this study.

Note that the IGBT used in the electrical model has a discrete package. This component was chosen because it makes sense in a string converter of this size. However, the CIPS08 model is originally made for modules. The CIP08 model is chosen because it extends to high cycle fatigue and has the most parameters. This is not seen as a problem because this work aims for a comparative study and not for absolute lifetime predictions for a specific system. The equation is as follows:

$$N_f = A^{\alpha} \cdot \Delta T_j^{\beta_1} \cdot \exp\left(\frac{\beta_2}{T_{j,min}+273.15}\right) \cdot t_{on}^{\beta_3} \cdot I^{\beta_4} \cdot V^{\beta_5} \cdot D^{\beta_5} \tag{3}$$

With N_f the number of cycles to failure, A, β_1, β_2, β_3, β_4, β_5 constant model parameters, ΔT_j the junction temperature fluctuation, $T_{j,min}$ the cycle minimum temperature, t_{on} the cycle heating time, I the current per bond wire, V the blocking voltage of the chip and D the bond wire diameter.

Next, this model needs to be extended to include high cycle fatigue. This model modifies the β_1 parameter of the original model to include high cycle fatigue [25]. Equation (4) shows the modified β_1. Fig. 8 shows the cycles to failure predicted

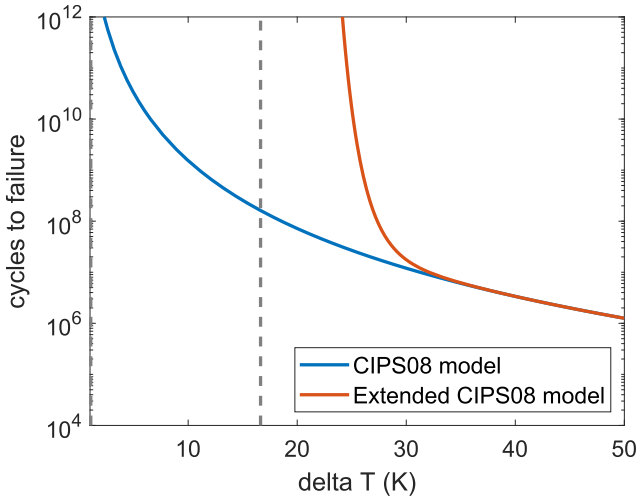

FIGURE 8. Cycles to failure predicted by CIPS08 and extended CIPS08 model for low delta T.

by the CIPS08 and extended model.

$$\beta_1' = \beta_1 + \exp(-\frac{\Delta T_j - 26.2\ K}{1.74\ K}) \tag{4}$$

The CIPS08 model requires cycle information in order to calculate cycles to failure. The junction temperature mission profile is broken up into a finite set of cycles using rainflow counting [29], [30], [31], [32], [33]. Finally, the individual cycles to failure are combined using Miners rule to calculate the total damage as shown in (5) [34]. Here k is the total amount of unique cycles, n_i is the occurrence of the cycle, and C is the total lifetime consumption.

$$\sum_{i=1}^{k} \frac{n_i}{N_i} = C \tag{5}$$

III. RESULTS

There are infinite possibilities for creating a solar-wind hybrid plant. Location, weather, park layout, and other factors will all influence the cast shadow. It is, therefore, important to define a case study but still provide some freedom to test different scenarios. In this study, a fictional park located in Hasselt, Belgium, is designed. Fig. 9 shows the complete park. The distance $D1$ between turbines is 150 m, and the distance $D2$ in the main wind direction is 250 m. In this study, 13 wind turbines are considered. The turbine rotors have a diameter of 55 m and a hub height of 65 m. Note how turbines north of the string are omitted since they cannot cast a shadow. The PV string will be located inside the PV string zone. This zone also contains one turbine that will be used as a reference to place the 28 PV panels. The PV panels have a dimension of 1 m by 2 m.

This work will compare multiple cases in the described hybrid plant and compare the IGBT lifetime and PV-energy yield with a reference case. This reference case is the PV system in the absence of wind turbines and thus, no shadow

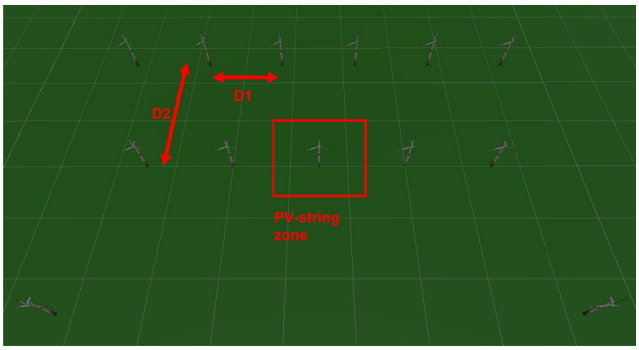

FIGURE 9. Wind park scene in unity.

scenarios. This reference case has the MPPT update speed set at 80 ms.

A. STATIC AND DYNAMIC SIMULATIONS

In this section, the Energy Yield and IGBT lifetime predictions from a static (no blade rotation) and dynamic (blade rotation) simulation are compared. Because in the static case, the shadow depends on the turbine blade position, 2 cases are defined where the blades are rotated with different angles as shown in Fig. 10. The PV string is placed 30 m and 50 m north of the wind turbine, and the MPPT update speed is set at 80 ms. The turbine blades rotate at 90 s^{-1} in the dynamic cases. Fig. 11 (a) shows the energy yield and lifetime compared to the reference case, and (b) the damage contribution and amount of cycles in function of junction delta T. In the 30 m dynamic simulation, a small bump is seen between 23 $°C$ and 32 $°C$ on the damage distribution. This indicates only a $\sim$ 1.2% of total damage is directly from shadow flicker-induced temperature swings. In the static cases, the blade orientation can influence the predicted lifetime and yield, with static-2 producing $\sim$ 2% worse results than static-1. The lifetime difference between static and dynamic is much larger at 13.2%, with the turbine scenario even experiencing an increased lifetime, but energy yield does see a drop of 1.3% compared to static orientation 1. The differences in lifetime and energy yield for the 50 m cases are much less pronounced. The dynamic case produces a 2% lower energy yield than static-2 produces. There is no big difference in lifetime between static and dynamic, as observed in the 30 m cases. It can be concluded that the energy yield and IGBT lifetime can vastly differ between static and dynamic simulations, but it seems to be case-dependent. The difference is also not directly caused by the additional temperature swings.

B. VARIABLE WIND TURBINE ROTOR AND MPPT UPDATE SPEED

The previous section shows that dynamic behavior can influence lifetime and energy yield compared to static cases. Because this difference is not directly caused by the additional temperature swings, an additional investigation is required into how the MPPT reacts to the shadow flicker.

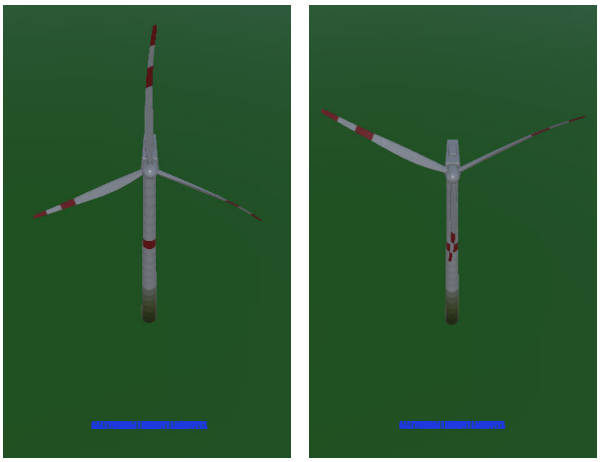

(a) (b)

FIGURE 10. Static case: (a) static-1 and (b) static-2. The turbine is located south of the PV string.

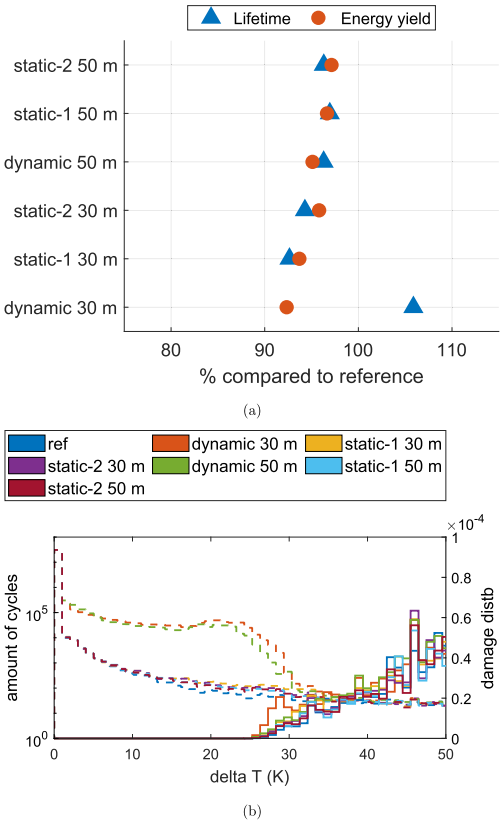

FIGURE 11. (a) Energy yield and IGBT lifetime compared to reference. (b) Amount of cycles (dotted) and damage distribution (full) for static and dynamic simulations.

This section investigates the effect of turbine rotor speed and MPPT update speed on lifetime and energy yield. For all cases studied in this section, the PV string is placed 30 m north of the wind turbine as shown in Fig. 10.

Fig. 12 shows a segment of the string voltage for July 9 for (a) multiple rotor speeds and (b) for multiple MPPT speeds. For the rotor speed comparison, the MPPT update

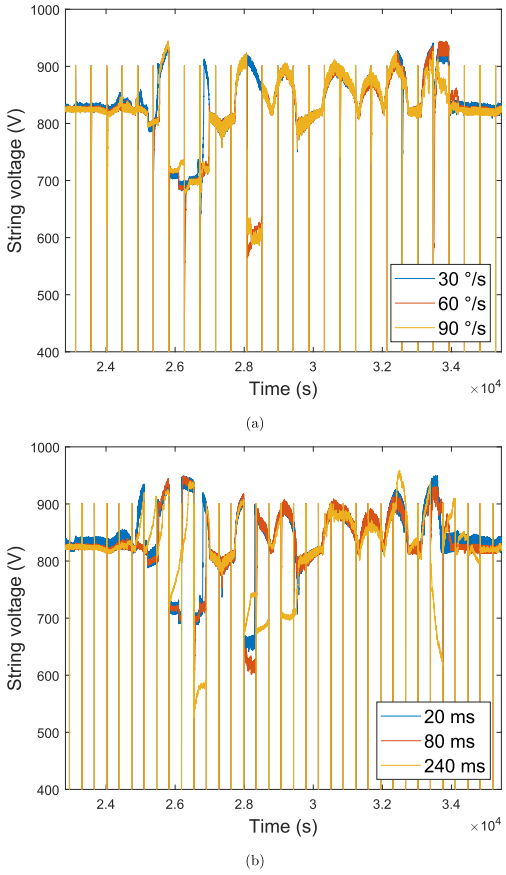

FIGURE 12. Voltage segment of July 9 for (a) multiple turbine rotor speed and (b) multiple controller MPPT speeds.

speed is kept at 80 ms. The rotor speed in the MPPT tracker comparison is kept at $90°s^{-1}$. The vertical lines are produced during the IV-sweep to find global MPP. Note that in all cases, irradiance, diffuse irradiance, and static turbine shade are identical. It is clear that string voltage can vary greatly depending on the rotor and MPPT speeds with specific intervals where string voltages vary greatly, possibly because the shadow flicker and rapidly changing IV-curve prohibits the proper functioning and MPPT. There can be multiple explanations. Firstly, because of the discrete sampling of the MPPT, the update interval can become in sync with the shadow flicker. Secondly, the tracker can be too slow to track MPP in these fast varying conditions, causing it to drift, move slowly, or get stuck. Additionally, shadow flicker happens during the global search, which can cause the tracker to choose a faulty global maximum from where the MPPT must escape.

Fig. 13 shows the lifetime, energy yield, and damage distributions for varying rotor speeds. Again the damage directly caused by temperature swings is $< 1\%$, but there are differences in lifetime between the cases. $30°s^{-1}$ and $90°s^{-1}$ perform better than the reference case, but the $60°s^{-1}$ performs similar. The impact on energy yield is minimal. The lifetime, energy yield, and damage distributions for the different MPPT speeds are shown in Fig. 14. Tracker

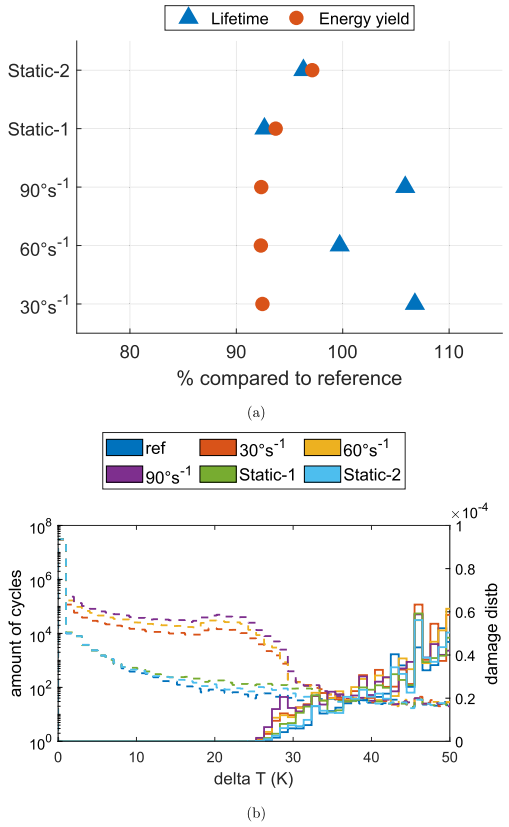

FIGURE 13. (a) Energy yield and IGBT lifetime compared to reference. (b) Amount of cycles (dotted) and damage distribution (full) for multiple wind turbine rotor rotation speeds.

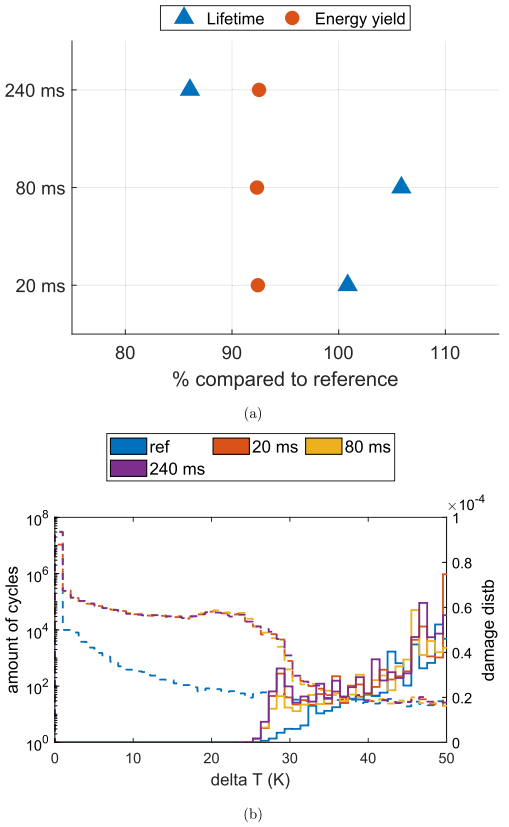

FIGURE 14. (a) Energy yield and IGBT lifetime compared to reference. (b) Amount of cycles (dotted) and damage distribution (full) for multiple MPPT update speeds.

speed can have a significant impact on lifetime, with the 80 ms tracker outperforming the 240 ms and 20 ms trackers. The lifetime seems to be extremely dependent on the rotor and MPPT speed. The MPPT has difficulty tracking MPP. It is important to note that the assumption that the rotor speed is constant is unrealistic. In practice, the rotor speed fluctuates with changes in wind speed, which can result in less pronounced voltage variations.

C. VARIABLE STRING-TURBINE DISTANCE AND ORIENTATION

In this section, the effect of PV string-turbine distance and orientation on IGBT lifetime and energy yield is investigated. All locations and orientations in Fig. 15 are investigated for multiple distances D. During this study, the rotor speed is kept at $90°s^{-1}$ and the MPPT speed at 80 ms. Fig. 16 shows the cycle counts and damage distributions. Cases a and b contain the most cycles. This is to be expected, as the turbine is directly south of the PV string. These cases are also the only ones that contain noticeable additional damage in the 25-35 °C delta T interval directly caused by shadow flicker.

Fig. 17 shows the IGBT lifetime and energy yield compared to the reference case. Cases *"b"*, *"c"*, *"d"*, *"e"* and *"f"* all show a rising trend in IGBT lifetime and energy yield as the distance to the wind turbine increases. This is to be expected; at greater distances, less shadow is cast on

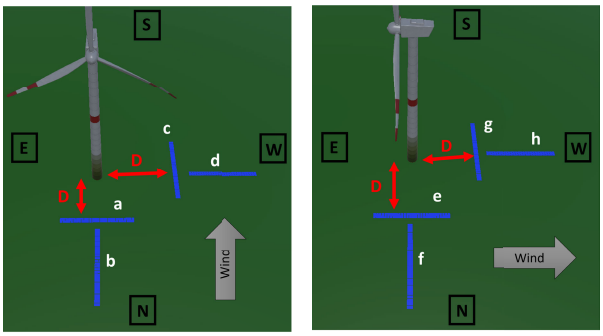

FIGURE 15. PV string zone with (a) North wind and (b) East wind.

the PV string. Case *"a"* forms a notable exception, with the lifetime at 30 m being a noticeable outlier from this trend. To explain this, all groups 2 and 3 cells are added up each day. The result is shown in Fig. 18. During summer, there is a dip because the sun is high in the sky except for the sting at 30 m. It seems that at this distance, the blades cast a "bad" shadow that covers a substantial amount of the PV string. During summer, solar irradiance and power are highest. This additional shadow can lower the strain on the IGBT during summer, thus greatly increasing lifetime.

Cases *"g"* and *"h"* have a minimal deviation from the reference case but experience a slight increase in

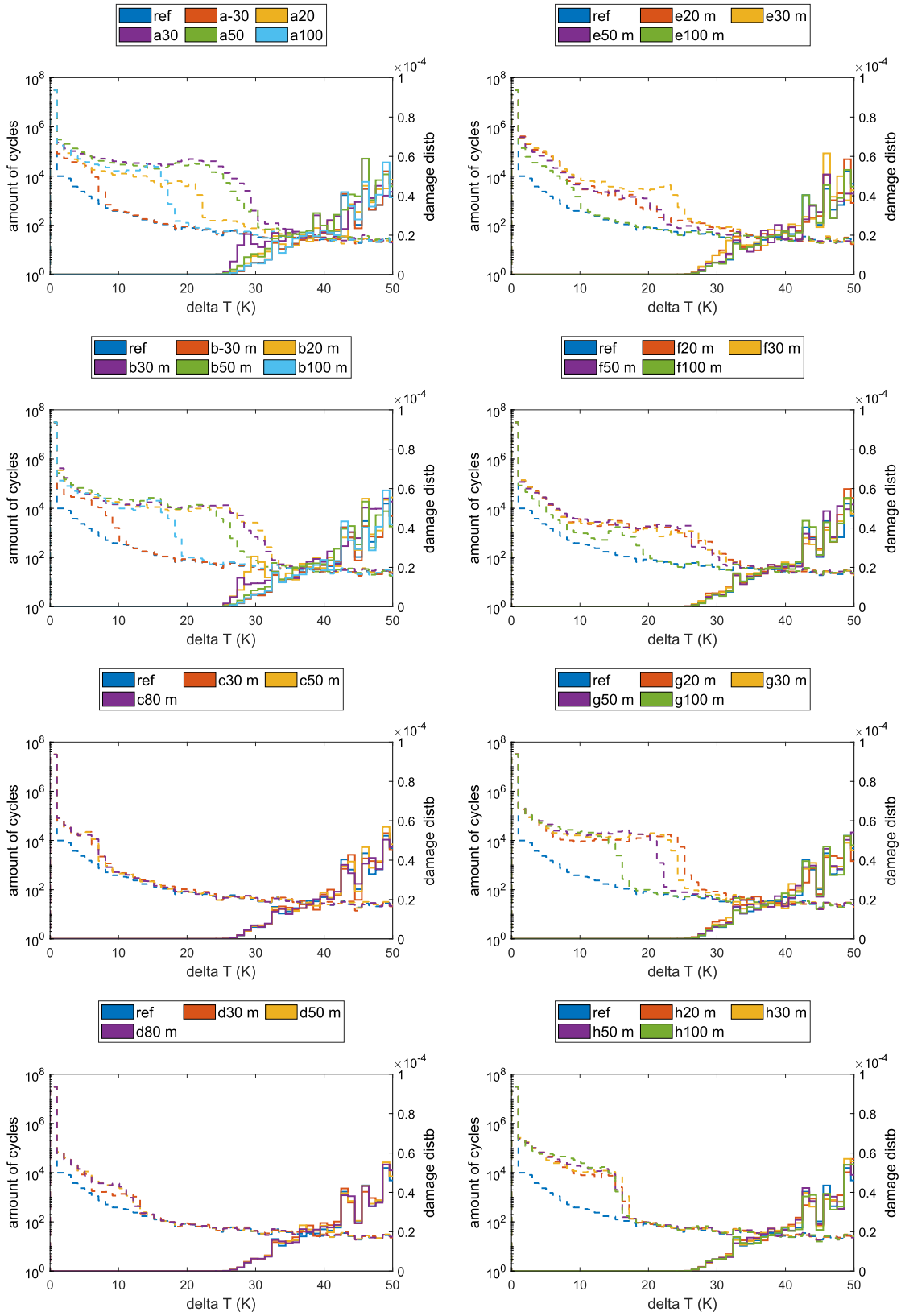

FIGURE 16. Amount of cycles (dotted) and damage distribution (full) for multiple locations and orientations for all locations in Fig. 15, followed by a number representing the distance *D*.

lifetime around 20 m-30 m. There is no direct explanation for this slight increase. It can possibly be a result of the MPPT reaction on shadow flicker as explained in section III-B.

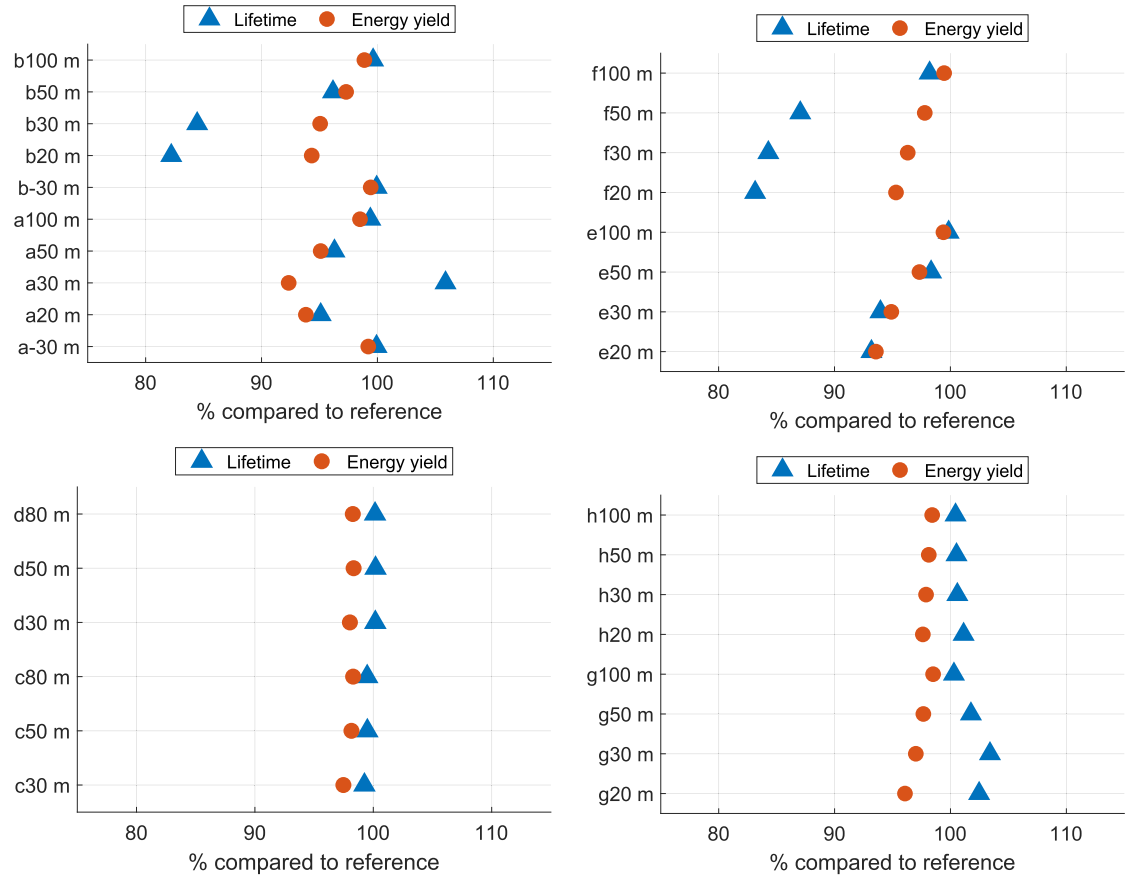

FIGURE 17. Energy yield and IGBT lifetime compared to reference for all locations in Fig. 15, followed by a number representing the distance *D*.

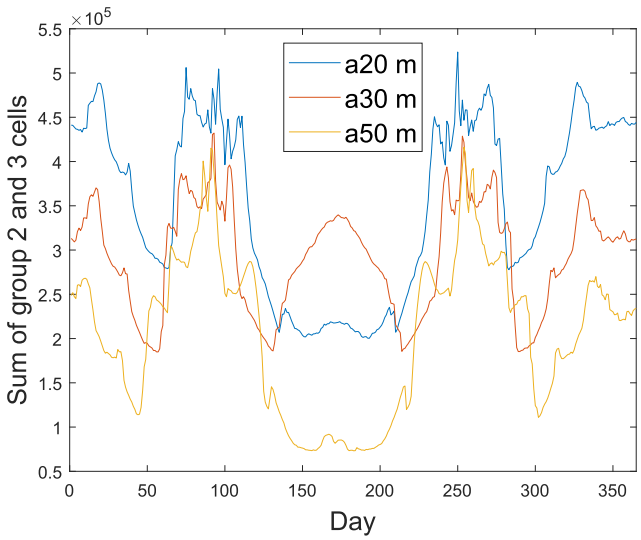

FIGURE 18. Sum of all group 2 and 3 cells for each day of the year.

Looking at the results from a design perspective, it seems that placing the PV string north of the wind turbine produces worse lifetimes, especially in the *"b"* and *"f"* orientations. The *"a"* and *"e"* orientations produce better lifetimes, but worse energy yields. PV strings are better placed more than 50 m south of the turbine. Eastern, western and northern orientations experience minimal influence of the wind turbine.

IV. CONCLUSION

This study investigates the effect of a wind turbine-induced shadow flicker on a PV system's energy yield and converter IGBT lifetime. This is done using a novel dynamic simulation methodology using Unity to calculate the shadows. First, it is concluded that there can be a significant difference in lifetime and yield between static and dynamic simulations. Even when performing static simulations, the blade position can produce different values for yield and IGBT lifetime. Dynamic simulations can thus be required to achieve more accurate energy yield and IGBT lifetime results, depending on the case. Further, wind turbine rotor speed and MPPT update speed can greatly influence yield and lifetime. It is shown that varying values of rotor speed and MPPT speed can cause variations in string voltages because the MPPT is unable to handle the shadow flicker and track the MPP. The problems MPPT can cause in shadow flicker scenarios are also seen in the work of Dekker et al. It is thus concluded that a good understanding of the MPPT and control loops is necessary to produce adequate yield and lifetime

predictions. Finally, the energy yield and IGBT lifetime are compared for multiple positions and orientations. The wind turbine can have a significant influence on lifetime and yield, so it is advised to place the PV string at least 50 m north of the wind turbine. Eastern, western, and southern string locations experience minimal influence from the wind turbine. Note that these conclusions are drawn for a fictional park in Belgium. Results can vary depending on location, park layout, wind turbine dimensions,…It is advised to evaluate the lifetime and yield on a case-to-case basis to make adequate yield and lifetime predictions. Future work could involve investigating alternative control schemes. It might be possible to minimize the effect of shadow flicker with specialized controllers. Additional measurements in real wind-solar hybrid farms are also recommended to observe controller reactions for different cases further. The presented study can also be expanded to look into different types of wind turbines and wind turbine dimensions. The importance of shadow flicker can also provide insight into other PV-integrated applications like vehicle-integrated PV. Vehicles can also experience rapidly moving shadows caused by passing trees and buildings;…These shadows can, as in the case of wind turbines, potentially influence the lifetime and energy yield.

REFERENCES

[1] (2024). *Renewables 2024 Global Status Report*. [Online]. Available: https://www.ren21.net/reports/global-status-report/

[2] O. Delbeke, J. D. Moschner, and J. Driesen, "The complementarity of offshore wind and floating photovoltaics in the Belgian north sea, an analysis up to 2100," *Renew. Energy*, vol. 218, Dec. 2023, Art. no. 119253, doi: 10.1016/j.renene.2023.119253.

[3] M. Ali, M. Riaz, M. A. Koondhar, M. S. Akram, J. M. Guerrero, J. C. Vasquez, and B. Khan, "Renewable energy sources-based hybrid microgrid system for off-grid electricity solution for rural communities," *Energy Sci. Eng.*, vol. 11, no. 10, pp. 3486–3499, Jul. 2023, doi: 10.1002/ese3.1535.

[4] A. Balal, R. Barnwal, and B. Yogi, "Designing a solar/wind hybrid power system for charging electric vehicles," in *Proc. IEEE Texas Power Energy Conf. (TPEC)*, Feb. 2023, pp. 1–5, doi: 10.1109/TPEC56611.2023.10078494.

[5] Y. Peng, S. Zhao, and H. Wang, "A digital twin based estimation method for health indicators of DC–DC converters," *IEEE Trans. Power Electron.*, vol. 36, no. 2, pp. 2105–2118, Feb. 2021, doi: 10.1109/TPEL.2020.3009600.

[6] A. Abuelnaga, M. Narimani, and A. S. Bahman, "A review on IGBT module failure modes and lifetime testing," *IEEE Access*, vol. 9, pp. 9643–9663, 2021, doi: 10.1109/ACCESS.2021.3049738.

[7] H. Ye, M. Lin, and C. Basaran, "Failure modes and FEM analysis of power electronic packaging," *Finite Elements Anal. Design*, vol. 38, no. 7, pp. 601–612, May 2002, doi: 10.1016/s0168-874x(01)00094-4.

[8] *Dynamic Simulation of the Shading Cast By a Wind Farm on an Adjacent Photovoltaic Plant*, Eur. Photovoltaic Sol. Energy Conf. Exhib., Bilbao, Spain, 2021.

[9] D. Ludwig, C. Breyer, A. A. Solomon, and R. Seguin, "Evaluation of an onsite integrated hybrid PV-wind power plant," *AIMS Energy*, vol. 8, no. 5, pp. 988–1006, 2020, doi: 10.3934/energy.2020.5.988.

[10] M. Agrawal, B. Kumar Saxena, and K. V. S. Rao, "Feasibility of establishing solar photovoltaic power plants at existing wind farms," in *Proc. Int. Conf. Smart Technol. For Smart Nation (SmartTechCon)*, Aug. 2017, pp. 251–256, doi: 10.1109/SMARTTECHCON.2017.8358378.

[11] P.-Y. Yin, C.-Y. Cheng, H.-M. Chen, and T.-H. Wu, "Risk-aware optimal planning for a hybrid wind-solar farm," *Renew. Energy*, vol. 157, pp. 290–302, Sep. 2020, doi: 10.1016/j.renene.2020.05.003.

[12] S. R. Mohanrajan, D. Kavitha, and G. P. Kumar, "Effective planning and analysis of solar panels in the wind farm," in *Proc. 12th Int. Conf. Smart Grid (IcSmartGrid)*, May 2024, pp. 130–135, doi: 10.1109/icsmartgrid61824.2024.10578122.

[13] P. Kaliappan and M. P. Selvan, "Design and performance analysis of utility scale-grid connected hybrid wind-solar plant in an existing operational wind farm in India," in *Proc. IEEE 3rd Int. Conf. Electr. Power Energy Syst. (ICEPES)*, Jun. 2024, pp. 1–6, doi: 10.1109/ICEPES60647.2024.10653465.

[14] N. J. Dekker, L. H. Slooff, M. J. Jansen, G. de Graaff, J. Hovius, R. Jonkman, J. Zuurbier, and J. Pronk, "Wind turbine dynamic shading: The effects on combined solar and wind farms," *J. Renew. Sustain. Energy*, vol. 15, no. 6, p. 38, Nov. 2023, doi: 10.1063/5.0176121.

[15] L. Bhukya, N. R. Kedika, and S. R. Salkuti, "Enhanced maximum power point techniques for solar photovoltaic system under uniform insolation and partial shading conditions: A review," *Algorithms*, vol. 15, no. 10, p. 365, Sep. 2022, doi: 10.3390/a15100365.

[16] F. Liu, Y. Kang, Y. Zhang, and S. Duan, "Comparison of P&O and Hill climbing MPPT methods for grid-connected PV converter," in *Proc. 3rd IEEE Conf. Ind. Electron. Appl.*, Jun. 2008, pp. 1–12, doi: 10.1109/ICIEA.2008.4582626.

[17] A. Safari and S. Mekhilef, "Simulation and hardware implementation of incremental conductance MPPT with direct control method using cuk converter," *IEEE Trans. Ind. Electron.*, vol. 58, no. 4, pp. 1154–1161, Apr. 2011, doi: 10.1109/TIE.2010.2048834.

[18] V. Jately, B. Azzopardi, J. Joshi, B. Venkateswaran V, A. Sharma, and S. Arora, "Experimental analysis of Hill-climbing MPPT algorithms under low irradiance levels," *Renew. Sustain. Energy Rev.*, vol. 150, Oct. 2021, Art. no. 111467, doi: 10.1016/j.rser.2021.111467.

[19] K. M. Tsang and W. L. Chan, "Maximum power point tracking for PV systems under partial shading conditions using current sweeping," *Energy Convers. Manage.*, vol. 93, pp. 249–258, Mar. 2015, doi: 10.1016/j.enconman.2015.01.029.

[20] J. W. Kimball and P. T. Krein, "Discrete-time ripple correlation control for maximum power point tracking," *IEEE Trans. Power Electron.*, vol. 23, no. 5, pp. 2353–2362, Sep. 2008, doi: 10.1109/TPEL.2008.2001913.

[21] R. Leyva, C. Alonso, I. Queinnec, A. Cid-Pastor, D. Lagrange, and L. Martinez-Salamero, "MPPT of photovoltaic systems using extremum–seeking control," *IEEE Trans. Aerosp. Electron. Syst.*, vol. 42, no. 1, pp. 249–258, Jan. 2006, doi: 10.1109/TAES.2006.1603420.

[22] W. Hayder, D. Sera, E. Ogliari, and A. Lashab, "On improved PSO and neural network P&O methods for PV system under shading and various atmospheric conditions," *Energies*, vol. 15, no. 20, p. 7668, Jul. 2022, doi: 10.20944/preprints202207.0386.v1.

[23] L. Van Cappellen, O. Alavi, and M. Daenen, "The effect of heat sink thermal capacitance and resistance on predicted lifetime of switching devices in photovoltaic applications," in *Proc. IEEE 14th Int. Symp. Diag. Electr. Mach., Power Electron. Drives (SDEMPED)*, Aug. 2023, pp. 239–245, doi: 10.1109/SDEMPED54949.2023.10271460.

[24] L. Van Cappellen, M. Deckers, O. Alavi, M. Daenen, and J. Driesen, "A real-time physics based digital twin for online MOSFET condition monitoring in PV converter applications," in *Proc. 28th Int. Workshop Thermal Investigations ICs Syst. (THERMINIC)*, Sep. 2022, pp. 1–4, doi: 10.1109/THERMINIC57263.2022.9950636.

[25] C. Schwabe, N. Thönelt, J. Lutz, and T. Basler, "High cycle fatigue testing of silicon IGBT devices under application-close conditions," *IEEE Trans. Power Electron.*, vol. 38, no. 11, pp. 14516–14525, Nov. 2023, doi: 10.1109/TPEL.2023.3296269.

[26] W. Van De Sande, S. Ravyts, O. Alavi, P. Nivelle, J. Driesen, and M. Daenen, "The sensitivity of an electro-thermal photovoltaic DC–DC converter model to the temperature dependence of the electrical variables for reliability analyses," *Energies*, vol. 13, no. 11, p. 2865, Jun. 2020, doi: 10.3390/en13112865.

[27] W. Van De Sande, O. Alavi, P. Nivelle, J. D'Haen, and M. Daenen, "Thermo-mechanical stress comparison of a GaN and SiC MOSFET for photovoltaic applications," *Energies*, vol. 13, no. 22, p. 5900, Nov. 2020, doi: 10.3390/en13225900.

[28] R. Bayerer, T. Herrmann, T. Licht, J. Lutz, and M. Feller, "Model for power cycling lifetime of IGBT modules–various factors influencing lifetime," in *Proc. 5th Int. Conf. Integr. Power Electron. Syst.*, Mar. 2008, pp. 1–6.

[29] *Standard Practices for Cycle Counting in Fatigue Analysis*, Standard E1049—85, ASTM Int., 2017, doi: 10.1520/e1049.

[30] W. Van De Sande, S. Ravyts, A. Sangwongwanich, P. Manganiello, Y. Yang, F. Blaabjerg, J. Driesen, and M. Daenen, "A mission profile-based reliability analysis framework for photovoltaic DC–DC converters," *Microelectron. Rel.*, vols. 100–101, Sep. 2019, Art. no. 113383, doi: 10.1016/j.microrel.2019.06.075.

[31] W. Van De Sande, M. Daenen, K. Spiliotis, J. Gonçalves, S. Ravyts, D. Saelens, and J. Driesen, "Reliability comparison of a DC–DC converter placed in building-integrated photovoltaic module frames," in *Proc. 7th Int. Conf. Renew. Energy Res. Appl. (ICRERA)*, Oct. 2018, pp. 412–417, doi: 10.1109/ICRERA.2018.8566709.

[32] Y. Shen, H. Wang, Y. Yang, P. D. Reigosa, and F. Blaabjerg, "Mission profile based sizing of IGBT chip area for PV inverter applications," in *Proc. IEEE 7th Int. Symp. Power Electron. Distrib. Gener. Syst. (PEDG)*, Jun. 2016, pp. 1–8, doi: 10.1109/PEDG.2016.7527028.

[33] M. Deckers, L. Van Cappellen, G. Emmers, F. Poormohammadi, and J. Driesen, "Cost comparison for different PV-battery system architectures including power converter reliability," in *Proc. 24th Eur. Conf. Power Electron. Appl. (EPE ECCE Europe)*, Sep. 2022, pp. 1–11.

[34] M. A. Miner, "Cumulative damage in fatigue," *J. Appl. Mech.*, vol. 12, no. 3, pp. A159–A164, Sep. 1945, doi: 10.1115/1.4009458.

LEANDER VAN CAPPELLEN received the M.S. degree in electronics and ICT engineering, in 2020. He is currently pursuing the Ph.D. degree in energy systems engineering with Hasselt University, Hasselt, Belgium. Since 2020, he has been a Researcher with the Energy Systems Engineering (ESE) Group, IMO-IMOMEC. His current research interests include but are not limited to, power electronics reliability, condition monitoring, and renewable energies.

MARTIJN DECKERS (Graduate Student Member, IEEE) received the bachelor's and Master of Science degrees in electrical engineering from KU Leuven, where he is currently pursuing the Ph.D. degree in electrical engineering with the Electa Research Group, Electrical Engineering Department. Alongside this, he is a Teaching Assistant in courses on magnetic power transfer, electrical motors and drives, heat transfer, and fluid dynamics. His research interests include the reliability of power electronic switches and multiple input-output converter architectures.

KRISTOF ENGELEN received the M.Sc. and Ph.D. degrees in electrical engineering from KU Leuven, Belgium, in 2005 and 2019, respectively. In 2019, he joined the Electa Research Group, Department of Electrical Engineering (ESAT), KU Leuven, where he has since been involved in several power electronics-related projects. He has co-authored several international research articles.

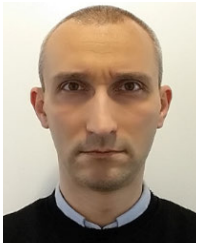

GEORGI H. YORDANOV was born in Bulgaria, in 1974. He received the M.Sc. degree in physics from the University of Sofia "St. Kliment Ohridski," in 1999, and the Ph.D. degree in electrical power engineering from the Norwegian University of Science and Technology (NTNU), in 2012. He has been a Technical Expert in PV energy meteorology with KU Leuven and Energy Ville, Belgium, since 2016. He has also been with the University of Agder (UiA), American College Arcus, Portellus Inc., JAR Computers, and the Bulgarian Academy of Sciences. His research interests include c-Si and thin-film (BI) PV, extreme solar over irradiance events (cloud enhancement), and high-performance computing.

MICHAËL DAENEN received the M.S. degree in applied physics from Technical University Eindhoven (TU/e), Eindhoven, The Netherlands, in 2004, and the Ph.D. degree in material physics from Hasselt University, Hasselt, Belgium, in 2008, on the topic of nanocrystalline diamond synthesis and characterization. Since 2014, he has been a Professor of engineering technology with Hasselt University. His research is spread over the wafer PV and module team and the energy system team at IMO-IMOMEC. He is the author of three U.S. patents and more than 80 papers published in high-quality journals and conferences. He focuses on the reliability of PV modules and PV systems and integrated PV, such as BIPV, IIPV, and Agri PV. He is also a reviewer for high-quality international journals and conferences.